

# Gravitational instability in protostellar disks at low metallicities

Kei E. I. Tanaka<sup>1,2</sup> \* and Kazuyuki Omukai<sup>1,2</sup> †

<sup>1</sup>*Astronomical Institute, Tohoku University, Sendai 980-8578, Japan*

<sup>2</sup>*Department of Physics, Kyoto University, Kyoto 606-8502, Japan*

28 February 2024

## ABSTRACT

Fragmentation of protostellar disks controls the growth of protostars and plays a key role in determining the final mass of newborn stars. In this paper, we investigate the structure and gravitational stability of the protostellar disks in the full metallicity range between zero and the solar value. Using the mass-accretion rates evaluated from the thermal evolution in the preceding collapse phase of the pre-stellar cores, we calculate disk structures and their evolution in the framework of the standard steady disks. Overall, with higher metallicity, more efficient cooling results in the lower accretion rate and lower temperature inside the disk: at zero metallicity, the accretion rate is  $\sim 10^{-3}M_{\odot} \text{ yr}^{-1}$  and the disk temperature is  $\sim 1000$  K, while at solar metallicity,  $\sim 10^{-6}M_{\odot} \text{ yr}^{-1}$  and  $\sim 10$  K. Despite the large difference in these values, the zero- and solar-metallicity disks have similar stability properties: the Toomre parameter for the gravitational stability, which can be written using the ratio of temperatures in the disk and in the envelope as  $Q_{\text{T}} \sim (T_{\text{disk}}/T_{\text{env}})^{3/2}$ , is  $\gtrsim 1$ , i.e., marginally stable. At intermediate metallicities of  $10^{-5} - 10^{-3}Z_{\odot}$ , however, the disks are found to be strongly unstable with  $Q_{\text{T}} \sim 0.1 - 1$  since dust cooling, which is effective only in the disks due to their high density ( $\gtrsim 10^{10} \text{ cm}^{-3}$ ), makes the temperature in the disks lower than that in the envelopes. This indicates that masses of the individual stars formed as a result of the protostellar disk fragmentation can be significantly smaller than their parent core in this metallicity range. The typical stellar mass in this case would be a few  $M_{\odot}$ , which is consistent with the observationally suggested mass-scale of extremely metal-poor stars.

**Key words:** early universe - stars: formation - stars: Population II - accretion, accretion disks.

## 1 INTRODUCTION

Stars in the early universe are considered to have played important roles in setting the environment for subsequent star formation in young galaxies, and starting the reionization and metal enrichment of the intergalactic medium through their radiation and kinetic energy injection in the supernovae (e.g., Ciardi & Ferrara 2005). Since the degree of those feedbacks strongly depends on the mass of stars, a number of studies have been carried out to pin down their mass range. Over the last decade, the first star formation from primordial pristine gas has been investigated in great depth, and their typical mass is found to be  $10 - 100M_{\odot}$  (McKee & Tan 2008; Hosokawa et al. 2011; Hirano et al.

2013). On the contrary, the initial mass function of present-day stars is observationally known to peak at  $\lesssim 1M_{\odot}$  in the solar neighborhood (Kroupa 2002; Chabrier 2003). These facts indicate the existence of a transition of the stellar mass-scale during the cosmic history.

A promising hypothesis is that this mass-scale transition has been caused by the fragmentation of pre-stellar clouds owing to the cooling by accumulated metals (Omukai 2000; Bromm et al. 2001; Schneider et al. 2002; Bromm & Loeb 2003; Omukai et al. 2005, 2010; Omukai 2012). In particular, for fragmentation into sub-solar mass clumps, rapid cooling at some high density, where the Jeans mass is small enough, is required. The cooling by dust thermal emission is considered to have played this role. Analytic studies (Schneider et al. 2003, 2006; Omukai et al. 2005, 2010) as well as numerical simulations (Clark et al. 2008; Dopcke et al. 2011, 2013) demonstrated that star-

\* E-mail: ktanaka@astr.tohoku.ac.jp

† E-mail: omukai@astr.tohoku.ac.jp

forming clouds enriched with metallicity above a critical value  $\sim 10^{-5}Z_{\odot}$  fragment at high density  $\gtrsim 10^{10}\text{cm}^{-3}$  by the dust cooling in the case of the same dust properties (i.e., depletion factor, size distribution, composition, etc.) as in the solar neighborhood. The critical metallicity remains at similar value even for models of the dust produced in the first-star supernovae although with some uncertainty, e.g., due to destruction by supernova reverse shocks, growth by coagulation during the pre-stellar collapse, etc. (Schneider et al. 2006, 2012; Nozawa et al. 2012; Chiaki et al. 2013)

So far, those studies have mainly focused on the fragmentation in the pre-stellar collapse, i.e., the preceding phase to the birth of protostars. The protostars, however, acquire most of their mass through disk accretion in the later so-called main-accretion phase. Low-mass clumps can thus be formed also by fragmentation of protostellar disks. In fact, even in the pristine-gas case, about  $\sim 1/2$  of the protostellar disks are found to fragment during the main-accretion phase, bearing low-mass clumps, according to numerical simulations (Stacy et al. 2010; Stacy & Bromm 2013). With increasing metallicity and thus enhanced dust cooling, the temperature in the disk will decrease. If the disk temperature becomes so low that the thermal pressure cannot cope with the disk self-gravity anymore, the disk will fragment into a number of smaller clumps. In the stellar cluster formed in this way, each member would be typically far less massive than their parent cloud. Here, to see the fragmentation properties of protostellar disks at low metallicities, we study their self-gravitational stability using the standard steady thin-disk prescription.

Some previous works have discussed the stability of low-metallicity disks with planet formation in low-metallicity environments in mind, and have concluded that they can be even more unstable than in the solar-metallicity disks (Cai et al. 2006; Meru & Bate 2010, see also Boss 2002). However, the metallicity range studied has been limited to rather high values of  $10^{-2} \lesssim Z/Z_{\odot} \lesssim 10$ , relevant to observed exoplanets. No comprehensive study has been carried out covering the entire metallicity range between zero and solar value. In addition, in those studies the initial disk structures were set up arbitrarily by hand. In reality, disk properties, such as the accretion rate and disk radius, depend on the metallicity of star forming gas, which determines the condition of accreting envelope. In this paper, we calculate the evolution of protostellar disks considering the accretion histories set by the structure of their parental clouds for the entire range of metallicities  $0 \leq Z \leq Z_{\odot}$ .

This paper is organized as follows. In Section 2, we describe the standard steady disk model adopted in this study. In Section 3, to extract the effect of different metallicity on the disk stability, we present the disk structures for given accretion rates and disk radii. Next, in Section 4, we illustrate evolution of the disks under accretion rates set by the pre-stellar collapse with various metallicities. In Section 5, we discuss roles of disk fragmentation on setting the final mass of stars formed and uncertainties in our model. Finally, we summarize our study in Section 6.

## 2 STEADY DISK MODEL

We here describe our model for the protostellar disks. Although the protostellar disks, especially in their early phase, evolve dynamically both in zero- (Stacy et al. 2010; Clark et al. 2011; Vorobyov et al. 2013) and the solar-metallicity cases (Walch et al. 2009; Vorobyov & Basu 2010; Machida et al. 2010; Tsukamoto & Machida 2011), we adopt the conventional steady-state  $\alpha$ -disk prescription (Shakura & Sunyaev 1973) to explore disk properties in a wide range of parameters (metallicity, stellar mass, disk radius, and accretion rate). We calculate the disk structure considering the gravity only from its central star, and then discuss its stability against the disk self-gravity. We use the Toomre parameter for the self-gravitational stability (Toomre 1964),

$$Q_{\text{T}} = \frac{c_s \kappa_{\text{ep}}}{\pi G \Sigma}, \quad (1)$$

where  $\kappa_{\text{ep}}$  is the epicycle frequency,  $\Sigma$  the disk surface density,  $c_s = \sqrt{k_{\text{B}}T/\mu m_{\text{H}}}$  the sound speed,  $T$  the temperature at the midplane,  $\mu$  the mean molecular weight,  $k_{\text{B}}$  the Boltzmann constant,  $m_{\text{H}}$  the proton mass, and  $G$  the gravitational constant. The epicycle frequency is given by the Keplerian angular velocity,  $\kappa_{\text{ep}} = \Omega_{\text{Kep}} \equiv \sqrt{GM_*/r^3}$ , where  $M_*$  is the stellar mass and  $r$  is the orbital radius. The disk structure with  $Q_{\text{T}} < 1$  is unstable for self-gravity and will fragment into clumps.

Let us consider the density and thermal structure of a disk with accretion rate  $\dot{M}$ . The density structure is determined by hydrostatic equilibrium in the vertical direction, and the mass and angular momentum conservation. From the vertical hydrostatic equilibrium,  $c_s^2/H = GM_*/r^3$ , the disk scale height  $H$  at the radius  $r$  is

$$H = \frac{c_s}{\Omega_{\text{Kep}}}. \quad (2)$$

In the innermost region of  $r \lesssim 1\text{AU}$ , the temperature can exceed  $T \gtrsim 10^5\text{K}$  and the radiation pressure can be important (Tanaka & Nakamoto 2011). We here, however, neglect the contribution of radiation pressure since we are interested in the disk structure and stability in the larger scale. The disk surface density  $\Sigma$  is evaluated from the assumption of steady accretion,

$$\Sigma = \frac{\dot{M}}{3\pi\nu}, \quad (3)$$

where  $\nu$  is the kinematic viscosity (e.g., Pringle 1981).

The thermal structure of the disks is determined by the thermal equilibrium at each radius

$$\mathcal{H} = \mathcal{L}, \quad (4)$$

where  $\mathcal{H}$  and  $\mathcal{L}$  are heating and cooling rate, respectively, per unit surface area. We consider the heating owing to the turbulent viscosity:

$$\mathcal{H} = \frac{9}{4}\nu\Sigma\Omega_{\text{Kep}}^2. \quad (5)$$

The heating by the stellar radiation is not included in the calculation and its influence will be discussed later in Section 5.2. As cooling processes, we consider radiative cooling by the  $\text{H}_2$  lines and the dust and gas continuum. Using the cooling rate per unit volume  $\Lambda$ , the surface cooling rate can

be written as

$$\mathcal{L} = 2H\Lambda. \quad (6)$$

The H<sub>2</sub>-line cooling rate is calculated as in Omukai et al. (2005) by solving rovibrational level populations for given H<sub>2</sub> column density. The most hydrogen is already in the molecular form in the disks due to the high density (typically  $\gtrsim 10^{10} \text{ cm}^{-3}$ ). We just assume that the gas is fully molecular and do not solve the chemical reaction equations. Although the cooling by H<sub>2</sub>O, HD, and CO lines as well as by fine-structure lines of [C I], [C II], and [O I] can be important in some density and metallicity ranges in the pre-stellar collapse phase, the dominant coolant in the high density range as in protostellar disks is always either H<sub>2</sub> or the continuum (Omukai et al. 2005, 2010). The continuum cooling rate by the gas  $\kappa_{g,i}$  and dust  $\kappa_{d,i}$ , where the subscript  $i=P,R$  means the Planck and Rosseland mean, respectively:

$$\Lambda_{\text{cont}} = \frac{4\sigma_{\text{SB}}\rho}{1+x} (\kappa_{g,P}T^4 + \kappa_{d,P}T_d^4), \quad (7)$$

$$x = \tau_P + 3\tau_R\tau_P/4, \quad (8)$$

$$\tau_i = (\kappa_{g,i} + \kappa_{d,i})\Sigma, \quad i = P, R. \quad (9)$$

where  $\sigma_{\text{SB}}$  is the Stefan-Boltzmann constant,  $\rho = \Sigma/(2H)$  the density,  $T_d$  the dust temperature, and  $\tau_{P,R}$  the optical depth. The function  $x(\tau_i)$  gives the correct limiting values both in the optically thin and thick regimes and smoothly connects them. For the gas opacity, we use that for the primordial gas by Mayer & Duschl (2005). We use the dust opacity by Semenov et al. (2003) in the solar metallicity case, which is reduced in proportion to the metallicity in other cases.

The dust temperature  $T_d$  is calculated from the energy balance between the dust thermal emission and energy transfer by collisions with gas particles:

$$4\sigma\rho\kappa_{d,P}(T_d^4 - T_{\text{rad}}^4) = \frac{n_d(2k_B T - 2k_B T_d)}{t_{\text{coll}}}, \quad (10)$$

where  $T_{\text{rad}}$  is the temperature of radiation field inside the disk,  $n_d$  the dust number density, and  $t_{\text{coll}}$  the mean free time between the collisions (Hollenbach & McKee 1979; Schneider et al. 2006). The radiation temperature is given by

$$T_{\text{rad}}^4 = \frac{x}{1+x} \frac{\kappa_{g,P}T^4 + \kappa_{d,P}T_d^4}{\kappa_{g,P} + \kappa_{d,P}}, \quad (11)$$

(See Appendix B4 of Omukai 2001, for derivation). The factor  $x/(1+x)$  on right-hand side is valid both in the optically thin and thick limits and connects them smoothly. Note that, in the energy-balance equation (eq. 10), both the dust opacity  $\kappa_{d,P}$  on the right-hand side and the dust number density  $n_d$  on the left-hand side being proportional to the metallicity, the dust temperature is independent of the metallicity. The dust and gas thermally couple above the density

$$n_{H,tc} \simeq 2.3 \times 10^{11} \left( \frac{T}{100\text{K}} \right)^{4.5} \text{ cm}^{-3} \quad (12)$$

(see Appendix A for the derivation), while the dust temperature is much lower than the gas temperature below  $n_{H,tc}$ .

We treat the transport of angular momentum by means

of viscosity with the  $\alpha$ -parameter

$$\nu = \alpha c_s H, \quad (13)$$

(Shakura & Sunyaev 1973). We divide  $\alpha$  into two components, those by the gravitational instability (GI) and by the magnetic rotational instability (MRI):  $\alpha = \alpha_{\text{GI}} + \alpha_{\text{MRI}}$ . It is known that the torque due to the gravitational instability is significant in protostellar disks (Bate 1998; Krumholz et al. 2009; Clark et al. 2011; Kuiper et al. 2011). The gravitational torque is efficient when the disk is marginally stable with  $Q_T \lesssim 1.5$ . This efficient torque prevents the disk from becoming too unstable. Once the Toomre parameter becomes less than unity by efficient cooling or high surface density, the disk fragments. In order to mimic such behavior of the gravitational-torque efficiency,  $\alpha_{\text{GI}}$  is often treated as a functional form of  $Q_T$  (Lin & Pringle 1987; Nakamoto & Nakagawa 1994, 1995; Kratter et al. 2008; Rice & Armitage 2009; Zhu et al. 2009; Takahashi et al. 2013). We also apply the following formula with which  $\alpha_{\text{GI}}$  increases abruptly around  $Q_T = 1.5$  and saturates at maximum value of at around  $Q_T = 1$ ,

$$\alpha_{\text{GI}} = \alpha_{\text{GI,max}} \exp(-Q_T^{10}/10), \quad (14)$$

where  $\alpha_{\text{GI,max}}$  is the maximum value of  $\alpha_{\text{GI}}$ . Various star formation simulations showed that  $\alpha$  can be as large as 0.1 – 1 via the gravitational torque (Krumholz et al. 2007; Kratter et al. 2010; Clark et al. 2011; Kuiper et al. 2011). Thus, we set  $\alpha_{\text{GI,max}} = 1$  as our reference value. However, the exact value of maximum  $\alpha$  is still controversial. Numerical simulations of isolated disks without infalling flow from the envelope suggested smaller maximum  $\alpha$  of 0.07 (Gammie 2001; Rice et al. 2005). While the star formation simulations follow every stages in star formation from the cloud cores, the isolated disk simulations are well controlled for extracting the fundamental physics of fragmentation. Our study cannot tell which maximum  $\alpha$  value is more feasible. Therefore, we also show the disk stability adopting the maximum  $\alpha$  of 0.07 to see the dependence on its value. When the disk is gravitationally stable ( $Q_T \gtrsim 1.5$ ), the MRI viscosity dominates the angular momentum transfer, for which we apply a fixed value of  $\alpha_{\text{MRI}} = 0.01$  (Davis et al. 2010; Shi et al. 2010). We should note that, in reality,  $\alpha_{\text{MRI}}$  varies depending on the ionization degree of the disk gas. Especially, in the “dead zone” where the ionization degree is too low to activate MRI,  $\alpha_{\text{MRI}}$  would be zero (Gammie 1996; Sano et al. 2000; Bai 2011). However, the choice of the  $\alpha_{\text{MRI}}$  value does not affect our conclusion, since the protostellar disks we are interested in are usually marginally or strongly unstable with  $Q_T \lesssim 1.5$ . We will discuss the uncertainty of  $\alpha_{\text{GI}}$  and  $\alpha_{\text{MRI}}$  and its influences on our conclusion in Section 5.2.

We should note that our steady-disk framework is unable to describe the dynamics of fragmentation process and its outcome. We apply the pseudo-viscosity  $\alpha = \alpha(Q_T)$ , which corresponds to the strength of turbulence. In fact, numerical simulations by Cossins et al. (2009) showed that the amplitude of turbulence in a self-gravitating disk is a function of the cooling rate rather than the Toomre parameter: the turbulent amplitude is regulated to produce heating rate that balances the cooling rate to maintain the disk in a marginally stable state. If the cooling rate is too high, the required turbulent amplitude enters into the non-linear

regime. Then, the Toomre parameter drops locally  $Q_T < 1$  and the disk fragments. This underlying physics of fragmentation is not strictly captured by our model, which treats the turbulence by the viscous parameter  $\alpha(Q_T)$ . However, our model is still appropriate to study the disk stability by the following reasons. First, the viscous heating is consistently regulated to balance the cooling (eq. 4). Second, our  $\alpha(Q_T)$  prescription is chosen in order to mimic that fragmentation occurs when the turbulent amplitude becomes too large:  $Q_T < 1$  once  $\alpha$  reaches the maximum (eq. 14). Additionally, local fluctuations of  $Q_T$  in a self-gravitating disk are relatively small and thus the average  $Q_T$  is also almost close to unity when the disk fragments. Because of these facts, the obtained solution gives the reasonable description of the disk structure even with the subtle difference from the realistic fragmentation process. Note that, although a disk with  $Q_T < 1$  is expected to fragment, we will present the disk structure also in the cases with  $Q_T < 1$  as a guide for understanding the disk stability.

### 3 LOCAL DISK STRUCTURES FOR GIVEN RADII AND ACCRETION RATES

Both the disk radius and accretion rate depend on structure of the parent pre-stellar core and thus on the metallicity. In this section, however, to see how the dust cooling affects the disk structure and stability, we present the results for given radii  $r$  and accretion rates  $\dot{M}$ . For the solar metallicity case, similar studies have been carried out by Clarke (2009) and Cossins et al. (2010).

Figure 1 illustrates the Toomre parameter  $Q_T$  on the  $r$ - $\dot{M}$  planes for different metallicities with  $\alpha_{\text{GI,max}} = 1$ . Since  $M_*$  and  $r$  appear in equations for disk structure (eq. 1, 2, and 5) only through  $\Omega_{\text{Kep}} = \sqrt{GM_*/r^3}$ , we here introduce the reduced radius  $r(10M_\odot/M_*)^{1/3}$  and use it as the horizontal-axis variable. Curves with cross symbols indicate evolutionary tracks of the outer disk radii and the accretion rates for the protostellar disks, which will be discussed in Section 4.2. We can see that disks are marginally stable ( $1 < Q_T \lesssim 1.5$ ) for wide area of parameter space at every metallicity. This is due to self-regulation process in a self-gravitating accretion disk: if the disk becomes marginally unstable with  $Q_T \simeq 1.5$ , the turbulence boosts the viscous heating rate and the efficiency of the angular momentum transfer (i.e., through enhanced  $\alpha$  value in our prescription), which works to keep the disk from becoming too unstable (Bate 1998; Gammie 2001; Takahashi et al. 2013). It can also be recognized for all of the metallicities the Toomre parameter  $Q_T$  tends to be small in the upper-right regions in all panels, i.e., disks are more unstable with higher  $\dot{M}$  or at larger  $r$ . From the following expression for the Toomre parameter (eq. 1),

$$Q_T = \frac{3\alpha c_s^3}{GM} \simeq 4.8\alpha \left( \frac{T}{1000\text{K}} \right)^{3/2} \left( \frac{\dot{M}}{10^{-3}M_\odot\text{yr}^{-1}} \right)^{-1}. \quad (15)$$

where equations (2) – (13) have been used, we immediately see that, with higher accretion rate, the disk is more massive and thus more unstable. The dependence of  $Q_T$  on the radius  $r$  is through the disk temperature  $T$ , which is lower at larger  $r$ , since the gravitational potential is shallower and so the viscous heating rate is smaller there. In the innermost region of several AU, on the other hand, the disk remains stable

even with accretion rate as high as  $\gtrsim 10^{-3}M_\odot\text{yr}^{-1}$  owing to very high temperature ( $\gtrsim 10^4\text{K}$ ). With the increase of metallicity, enhanced dust-cooling rate makes the disk temperature lower and thus the unstable region extends toward lower accretion rate. Note that, in the  $10^{-5}$  and  $10^{-4}Z_\odot$  cases with  $\gtrsim 10^{-4}M_\odot\text{yr}^{-1}$ , the disk is more unstable in a region around 100AU (in terms of the reduced radius) than in the outer part around 1000AU. This is because the dense environment in the inner disk is needed to activate the dust cooling in such a low-metallicity environment. With more metals of  $10^{-3} - 1Z_\odot$ , the disk in the region of 10 – 100AU tends to be stabilized. This is because the disk is optically thick to the dust absorption and becomes stable owing to the resultant high temperature (Clarke 2009; Cossins et al. 2010).

In Figure 2, we present the disk stability at various metallicities adopting the maximum  $\alpha$  of 0.07, which is suggested by isolated disk simulations (Gammie 2001; Rice et al. 2005). At the solar metallicity, the fragmentation boundary agrees with those shown by Clarke (2009) and Cossins et al. (2010), who adopted the maximum  $\alpha \simeq 0.06 - 0.09$ . Comparing with the cases of  $\alpha_{\text{GI,max}} = 1$ , which is indicated from star formation simulations (Krumholz et al. 2007; Kratter et al. 2010; Clark et al. 2011; Kuiper et al. 2011), the marginally unstable region shrinks and the unstable region broadens. This is because the self-regulation effect by the gravitational torque is weaker for smaller maximum  $\alpha$ -value. As seen in equation (15), if temperature is constant, the critical accretion rate for  $Q_T = 1$  is inversely proportional to the maximum value of  $\alpha$ . In this way, the maximum  $\alpha$  value determines the efficiency of self-regulation and thus the fragmentation boundary of  $Q_T = 1$ . However, the general trends are same in both cases: disks are more unstable with higher accretion rates and larger radii for every metallicity, and unstable region extends toward lower accretion rate as the increase of metallicity and dust cooling efficiency. Therefore, we will show mainly the results with  $\alpha_{\text{GI,max}} = 1$  hereafter and discuss the influence of the uncertainty of  $\alpha$  value in Section 5.2.

We see the disk structure in the reference case, where  $M_* = 10M_\odot$ ,  $\dot{M} = 10^{-3}M_\odot\text{yr}^{-1}$ , and  $r = 100\text{AU}$  and its metallicity dependence in more detail. In both the primordial star formation (Stahler et al. 1986; Omukai & Nishi 1998; Abel et al. 2002; Bromm & Loeb 2004; Yoshida et al. 2006) and coincidentally in massive star formation in the local universe (e.g. Zinnecker & Yorke 2007), the typical accretion rate is  $\sim 10^{-3}M_\odot\text{yr}^{-1}$  and the disk radius is about  $\sim 100\text{AU}$  at  $10M_\odot$  (Tan & McKee 2004). Figure 3 shows the number density  $n_{\text{H}}$ , the gas and dust temperatures  $T$ , and  $T_{\text{d}}$  (*upper panel*), and the surface density  $\Sigma$ , the Planck and Rosseland-mean optical depths  $\tau_{\text{P}}$  and  $\tau_{\text{R}}$  (*lower panel*) in the reference case as functions of metallicity. Below metallicity  $10^{-5}Z_\odot$ , where the  $\text{H}_2$  line dominates the cooling, the gas temperature is constant at  $\sim 1000\text{K}$ , while the dust temperature remains about 200K, lower than the gas temperature. With metallicity exceeding  $10^{-5}Z_\odot$ , the dust thermal emission begins to dominate the cooling. The gas and dust thermally couple each other and have similar temperatures, which decrease with increasing metallicity until  $Z \simeq 10^{-3}Z_\odot$ . At this point, the optical depth reaches unity (bottom panel of Fig. 3). Note that the optical depth is roughly proportional to the metallicity since the surface

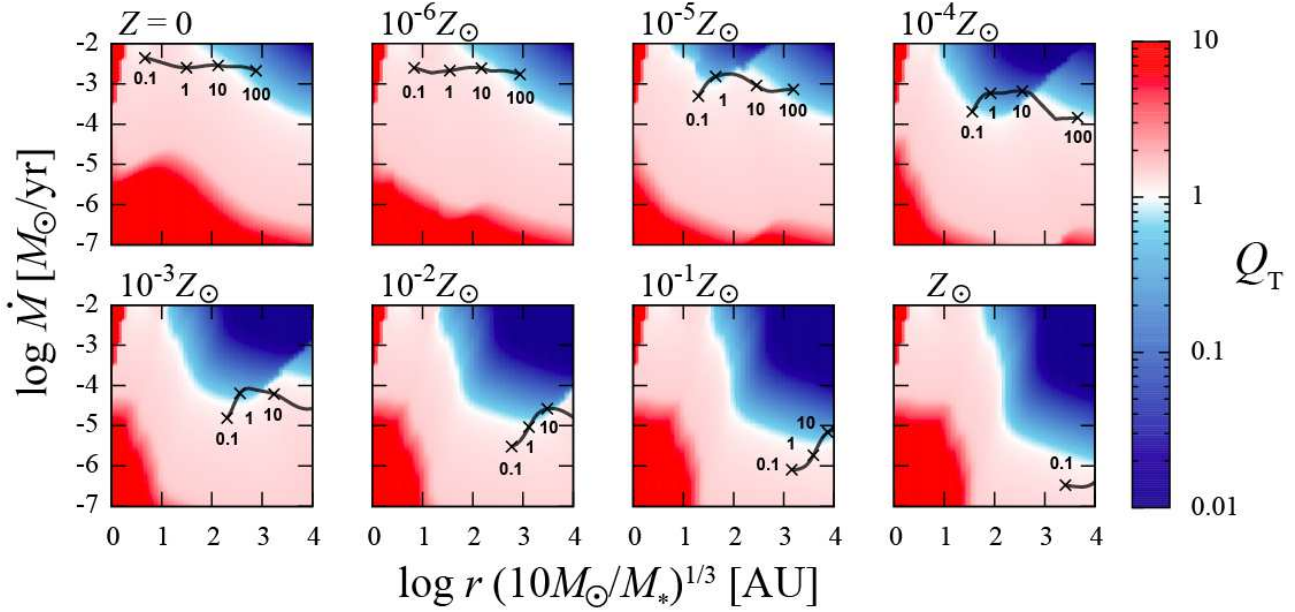


**Figure 1.** Gravitational stability of the disks with metallicities  $Z/Z_\odot = 0, 10^{-6}, 10^{-5}, 10^{-4}, 10^{-3}, 10^{-2}, 10^{-1},$  and  $1$  (from top-left to bottom-right) in the case of  $\alpha_{\text{GI,max}} = 1$ . In each panel, the Toomre parameter  $Q_{\text{T}}$  is indicated by color contours for given radii (horizontal axis) and accretion rates (vertical axis). Note that the reduced radius  $r(10M_\odot/M_*)^{1/3}$  is used on the horizontal axis (see text in Sec. 3). Curves illustrate evolutionary tracks of the outer disk radii  $r_{\text{d}}$  and accretion rates  $\dot{M}$  for the central protostellar mass  $M_* = 0.1 - 100M_\odot$ , and the crosses on them correspond to  $M_* = 0.1, 1, 10,$  and  $100M_\odot$  (see text in Sec. 4.2).

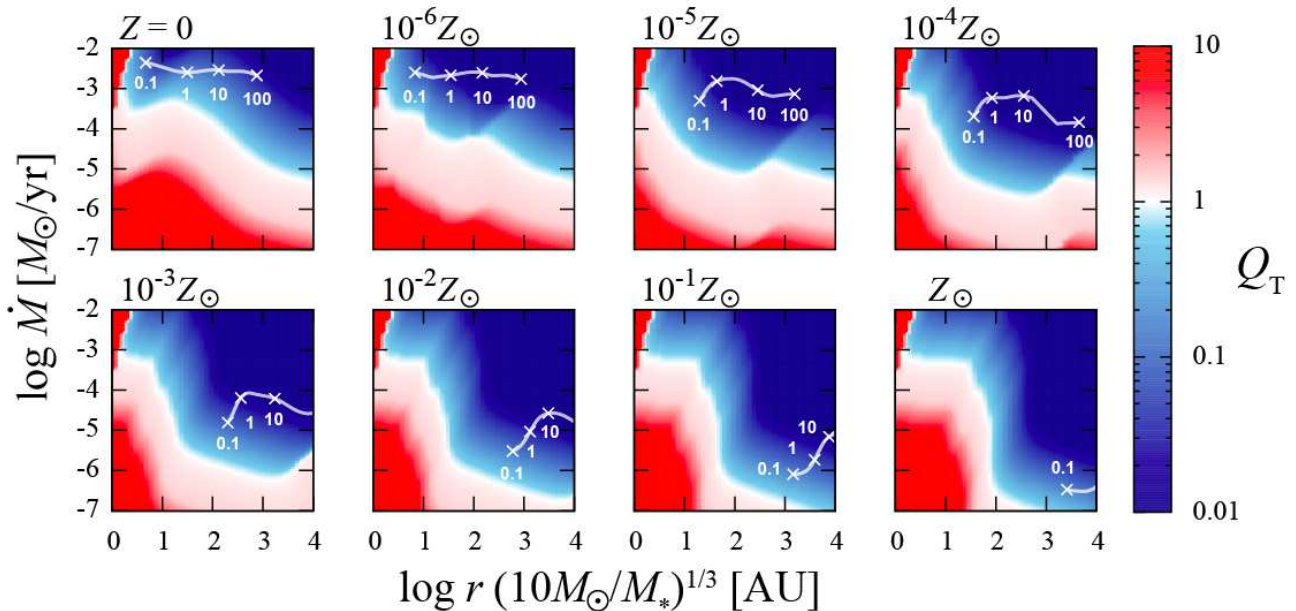


**Figure 2.** Same as Figure 1 except for the maximum  $\alpha$  of  $0.07$  ( $\alpha_{\text{GI,max}} = 0.06$  and  $\alpha_{\text{MRI}} = 0.01$ ).

density is relatively constant within an order of magnitude difference for different metallicities (bottom panel of Fig. 3). With higher metallicity  $Z \gtrsim 10^{-3}Z_\odot$ , the disk becomes optically thick and the radiative cooling becomes inefficient. Now the temperature turns up with metallicity. Even with the same  $M_*, \dot{M}$ , and  $r$ , the gas temperature varies with an order of magnitude depending on the metallicity. As seen in the upper panel of Figure 3, the number density  $n_{\text{H}}$  and the

gas temperature  $T$  behave in the opposite way in response to varying metallicity. This can be understood as follows: the lower temperature leads the smaller scale height (by eq. 2) and the higher surface density due to smaller viscosity (by eq. 3 and 13; bottom panel of Fig. 3), and thus the higher density. Note that the density is always higher than  $10^{11}\text{cm}^{-3}$ , which justifies our assumption of the fully molecular gas in this parameter range.

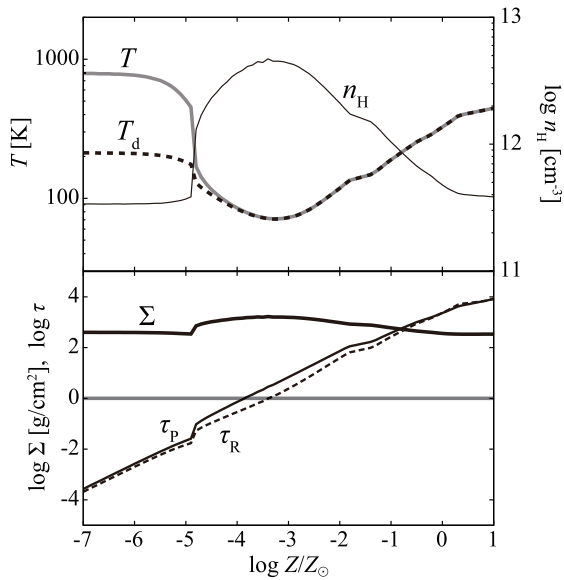


**Figure 3.** Metallicity dependence of local disk structure in the reference case where  $M_* = 10M_\odot$ ,  $\dot{M} = 10^{-3}M_\odot\text{yr}^{-1}$ , and  $r = 100\text{AU}$ . *Top:* the gas temperature  $T$ , the dust temperature  $T_d$ , and the number density  $n_H$ . *Bottom:* the surface density  $\Sigma$ , the Planck- ( $\tau_P$ ) and Rosseland-mean ( $\tau_R$ ) optical depths. The gray horizontal line in the bottom panel represents the optically thick/thin boundary of  $\tau = 1$ . The gas temperature reaches the minimum around  $\tau = 1$ . We should note that the structure for  $Z \simeq 10^{-5} - 1Z_\odot$  is unstable ( $Q_T < 1$ ; see Fig. 4) and our steady disk framework is not able to describe such an unstable structure self-consistently.

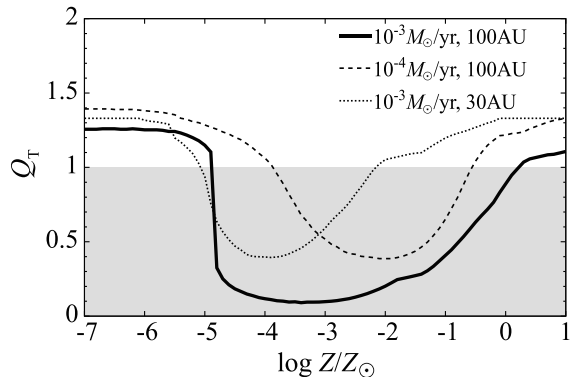


**Figure 4.** The Toomre parameter  $Q_T$  as a function of metallicity for the reference and two other cases for comparison. All cases are with  $M_* = 10M_\odot$ . The accretion rates and disk radii are: (i)  $10^{-3}M_\odot\text{yr}^{-1}$  and 100AU (it solid; the reference case), (ii)  $10^{-4}M_\odot\text{yr}^{-1}$  and 100AU (dashed), and (iii)  $10^{-3}M_\odot\text{yr}^{-1}$  and 30AU (dotted). Gray area indicates the instability domain against self-gravity ( $Q_T < 1$ ).

Figure 4 shows the metallicity dependence of the Toomre parameter  $Q_T$  in three cases including the reference one. From comparison between  $Q_T$  and  $T$  (top panel of Fig. 3) in the reference case ( $10^{-3}M_\odot\text{yr}^{-1}$  and 100AU), we find their metallicity dependences are very similar because  $Q_T \propto T^{3/2}$  (eq. 15). Like  $T$ ,  $Q_T$  also reaches the minimum  $\simeq 0.1$  at  $\tau \simeq 1$ . In reality, such an unstable disk would frag-

ment and could not continue accretion steadily. In Figure 4, two other cases are also shown: one with smaller accretion rate ( $10^{-4}M_\odot\text{yr}^{-1}$ ) and the other with smaller radius (30AU) than in the reference case. In all cases,  $Q_T$  values take the minimum around  $10^{-4} - 10^{-2}Z_\odot$ , although their quantitative values are different. In the case with lower accretion rate  $10^{-4}M_\odot\text{yr}^{-1}$ , the disk is less massive and less unstable than in the reference case ( $10^{-3}M_\odot\text{yr}$ ) as indicated by equation (14). In this case,  $Q_T$  takes its minimum at somewhat higher metallicity of  $10^{-2}Z_\odot$  than in the reference case ( $\sim 10^{-3}Z_\odot$ ) since the disk becomes optically thick only at higher metallicity due to the lower surface density. Also, at the more inner radius 30AU, the disk is less unstable than in the reference case (100AU) because the temperature is higher there due to the deeper gravitational potential. The minimum  $Q_T$  is attained at lower metallicity ( $\sim 10^{-4}Z_\odot$ ) than in the reference case because of the higher surface density at the smaller radius.

## 4 GLOBAL DISK STRUCTURE AND ITS EVOLUTION

In the previous section, we present the results for a wide range of the accretion rate  $\dot{M}$  and radius  $r$ . In realistic star-forming environments, both the accretion rate and the disk size depend on the properties of inflows from the envelope. The envelope structure is set up during the gravitational collapse of the parent pre-stellar core and depends on the metallicity. In this section, we construct models for infalling envelopes and calculate the protostellar-disk structures for given metallicities.

### 4.1 Model for infalling envelope

As in the standard scenario for present-day star formation, we here consider the collapse of a pre-stellar core from slightly gravitationally unstable state (Larson 1969; Shu 1977; Stahler, Shu, & Taam 1980). We also assume the core is spherically symmetric for simplicity since centrifugal force is not important in the region far outside the disk, which we are currently interested. The pre-stellar core undergoes so-called the runaway collapse: only the central densest part, which becomes smaller and smaller in mass, collapses significantly leaving outer less dense material almost unevolved. The size of the central part is roughly given by the instantaneous Jeans length and its collapse timescale is about the free-fall time. Eventually, a low-mass ( $\sim 0.01M_\odot$ ) protostar is formed at the center while most of the gas is left behind in the surrounding envelope. Because the density and temperature in the envelope remain almost unchanged after that portion of the gas is detached from the central part until the protostar formation at the center, the envelope structure can be constructed from the thermal evolution in the center part during the collapse. Omukai et al. (2005) investigated thermal evolution of the pre-stellar clouds during the collapse by way of a one-zone model, considering detailed chemical and radiative processes. This model provides us with the sound speed  $c_{s,1z}$  as a function of density  $\rho_{s,1z}$  for each metallicity. The radial mass distribution in the envelope is constructed assuming that inside the radius of the Jeans length  $R_{\text{env}} = c_{s,1z} \sqrt{\pi/G\rho_{1z}}$ , a Jeans mass of gas

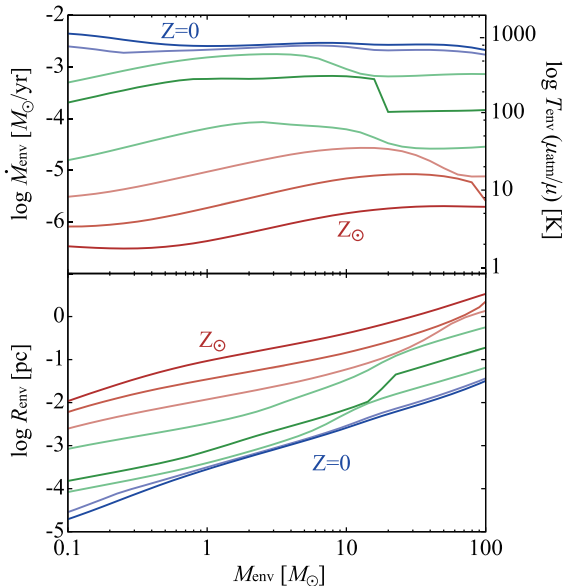


**Figure 5.** The envelope structures at various metallicities. The infall rate  $\dot{M}_{\text{env}}$  (top) and the radius  $R_{\text{env}}$  (bottom) are plotted as functions of the enclosed mass  $M_{\text{env}}$ . In the top (bottom) panel,  $Z/Z_{\odot} = 0, 10^{-6}$  (blue),  $10^{-5}, 10^{-4}, 10^{-3}$  (green),  $10^{-2}, 10^{-1}$ , and 1 (red) from top to bottom (from bottom to top, respectively). The envelope temperature  $T_{\text{env}}$  divided by the molecular weight  $\mu$  is indicated on the right vertical axis of the top panel. Here, the molecular weight is normalized with its value for the fully atomic gas  $\mu_{\text{atm}} \simeq 1.2$ .

$M_{\text{env}} = \rho_{1z} R_{\text{env}}^3$  is contained (Hosokawa & Omukai 2009). After the protostar formation at the center, the gas in the envelope starts accreting onto it. The infall rate from the envelope  $\dot{M}_{\text{env}}$  can be estimated from the enclosed mass  $M_{\text{env}}$  divided by the free-fall time  $t_{\text{ff}}$ , and given by

$$\dot{M}_{\text{env}} \simeq \frac{M_{\text{env}}}{t_{\text{ff}}} \simeq \frac{c_{s,1z}^3}{G}, \quad (16)$$

(Shu 1977). We regard this infall as hitting onto the outer disk edge and the accretion rate through the disk is constant of radius, i.e.,  $\dot{M} = \dot{M}_{\text{env}}$ , from the steady assumption. Note that the mass in the disk  $M_{\text{d}} \simeq \pi r_{\text{d}}^2 \Sigma(r_{\text{d}})$  is always small in comparison with the stellar mass: from equations (1) and (2), their ratio can be written as  $M_{\text{d}}/M_{\star} \simeq H/(r_{\text{d}} Q_{\text{T}})$ , which indicates that  $M_{\text{d}}/M_{\star} \simeq H/r \ll 1$  even in the case of a massive disk with  $Q_{\text{T}} = 1$ . Neglecting the mass in the disk, we set the instantaneous protostellar mass  $M_{\star}$  equal to the total accreted mass  $M_{\text{env}}$ .

Figure 5 shows the infall rate  $\dot{M}_{\text{env}}$  and the radius  $R_{\text{env}}$  as functions of the enclosed mass  $M_{\text{env}}$  for various metallicities. Recall that the infall rate depends only on the sound speed of the envelope gas,  $\dot{M}_{\text{env}} \propto c_{s,1z}^3 \propto (T_{\text{env}}/\mu)^{3/2}$  (eq. 16). On the right vertical axis of top panel in Figure 5,  $T_{\text{env}}/\mu$  is indicated, where  $\mu$  is normalized by its value for the fully atomic gas  $\simeq 1.2$ . Note the gas is almost atomic in the outer envelope with  $M_{\text{env}} \gtrsim$  a few  $M_{\odot}$ , while it is mostly molecular more inside with  $\mu \simeq 2.3$ . With metallicity as low as  $10^{-6} Z_{\odot}$ , the envelope structure deviates little from that of zero metallicity. With higher metallicity, the temperature in the envelope and so the infall rate become lower due to the cooling either by dust ( $\gtrsim 10^{-5} Z_{\odot}$ ) or by

metal lines ( $\gtrsim 10^{-4} Z_{\odot}$ ) (Omukai et al. 2005, 2010). The decrease of infall rate with metallicity can be roughly fitted as  $\dot{M}_{\text{env}} \sim 10^{-3} (Z/10^{-6} Z_{\odot})^{-0.5} M_{\odot} \text{yr}^{-1}$ . The higher temperature at lower metallicity results in the more compact infalling envelope: the envelope radius  $R_{\text{env}} \sim GM_{\text{env}}/c_{s,\text{env}}^2$  is smaller for the same enclosed mass.

We have constructed the envelope structure under the assumption of the spherical symmetry. In reality, however, materials in the envelope have non-zero angular momentum. As a result, a protostellar disk is eventually formed and the accretion proceeds onto the protostar through it. To evaluate the disk radius, we need to model the angular momentum distribution in the envelope. We parameterize the envelope rotation using the ratio of rotational velocity  $v_{\text{rot,env}}$  to the Keplerian velocity  $v_{\text{Kep,env}} = \sqrt{GM_{\text{env}}/R_{\text{env}}}$ :

$$f_{\text{Kep}} = \frac{v_{\text{rot,env}}}{v_{\text{Kep,env}}} \quad (17)$$

and assume it has a constant value in the envelope. In studies on the first star formation, this parameter has been found  $f_{\text{Kep}} \simeq 0.5$  without significant dependence on radius (Abel et al. 2002; Yoshida et al. 2006). We here adopt  $f_{\text{Kep}} = 0.5$  as the fiducial value, but also study a case of smaller value  $f_{\text{Kep}} = 0.25$  to see the effect of difference in rotation degree. The conservation of angular momentum in the infall leads to the disk outer radius

$$r_{\text{d}} = f_{\text{Kep}}^2 R_{\text{env}}. \quad (18)$$

## 4.2 Results

Figure 6 shows the protostellar-disk structure at four epochs  $M_{\star} = 0.1, 1, 10,$  and  $100 M_{\odot}$  for  $Z/Z_{\odot} = 0, 10^{-4},$  and 1 with the fiducial rotation parameter  $f_{\text{Kep}} = 0.5$ : top, middle, and bottom panels present the radial distributions of the temperature  $T(r)$ , the number density  $n_{\text{H}}(r)$ , and the Toomre parameter  $Q_{\text{T}}(r)$ , respectively. Recall here that, in Figure 1, the evolutionary tracks of the disk outer radii  $r_{\text{d}}$  and instantaneous accretion rates  $\dot{M}$  are indicated with curves with crosses.

First we see the zero-metallicity case (left column of Fig. 6). As the stellar mass increases, the disk becomes larger since the infalling gas has larger angular momentum. At more inner radius and with higher stellar mass, the temperature becomes higher owing to the deeper gravitational potential and thus higher viscous heating rate. At the optically thick innermost region of  $\lesssim 10 \text{AU}$ , the inefficient cooling makes the temperature very high and correspondingly the density low (top and middle panels). Outside  $10 \text{AU}$ , the temperature remains about  $300 - 3000 \text{K}$  by the  $\text{H}_2$ -line cooling. This disk temperature is similar to the envelope temperature, which is indicated with bars in top-left panel of Fig. 6 for each stellar-mass case. In the bottom-left panel of Figure 6, the Toomre parameter is almost constant at  $Q_{\text{T}} \simeq 1$  in a large part of the disk by the self-regulation process due to gravitational torque. In the outer disk of  $\sim 1000 \text{AU}$ , however, the Toomre parameter falls below unity since the temperature is too low for this self-regulation mechanism to compensate the instability. On the other hand, in the inner disk of a few AU, the high temperature results in very high  $Q_{\text{T}} (\gg 1)$ . As indicated by the evolutionary track ( $r_{\text{d}}, \dot{M}$ ) in the panel for the  $Z = 0$  case of Figure 1, the accretion

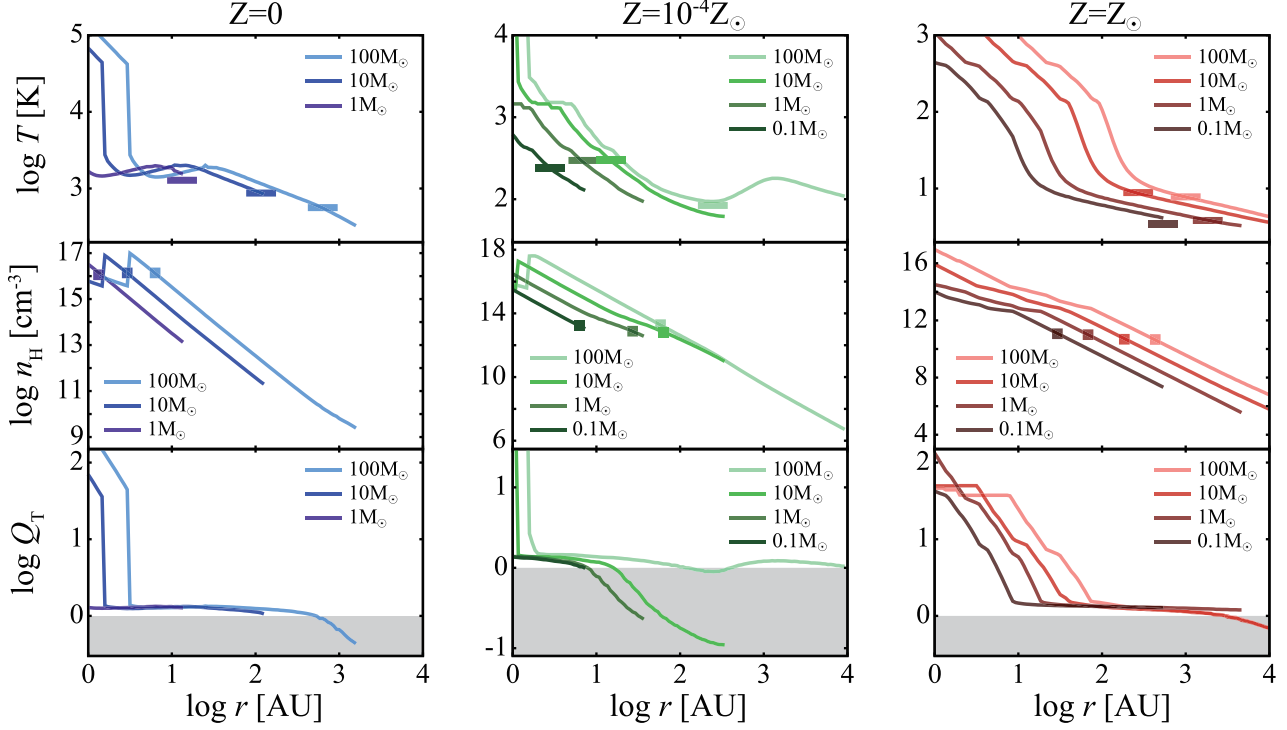


**Figure 6.** The radial structures of the protostellar disks and their evolution for metallicities  $Z/Z_{\odot} = 0, 10^{-4},$  and  $1$  (from left to right) with the fiducial rotation parameter  $f_{\text{Kep}} = 0.5$ . The distribution of temperature  $T$ , density  $n_{\text{H}}$ , and Toomre parameter  $Q_{\text{T}}$  are shown at protostellar masses of  $M_{*} = 0.1, 1, 10,$  and  $100M_{\odot}$  (in the  $Z = 0$  panel, the line for  $0.1M_{\odot}$  is not shown because the disk outer radius is smaller than  $1\text{AU}$ ). Thick bars in top panels indicate the envelope temperatures  $T_{\text{env}}$  in the corresponding epochs. Square symbols in middle panels show the radii where the Planck-mean optical depth is equal to unity. Gray areas in bottom panels represent the unstable region with  $Q_{\text{T}} < 1$ .

rate is always as high as  $\gtrsim 10^{-3}M_{\odot}\text{yr}^{-1}$  and the outer disk enters the unstable domain when  $\gtrsim 10M_{\odot}$ .

Next, we see the case of the disk with  $10^{-4}Z_{\odot}$  (middle column of Fig.6). In this case, the efficient dust cooling makes the temperature lower at  $100 - 1000\text{K}$  than the temperatures of the zero-metallicity disk. Also, the temperature at the outer disk falls below the envelope temperature shown by the bars. As a result, a large part of the disk becomes strongly unstable with  $Q_{\text{T}} = 0.1 - 1$  in the low-mass regime of  $1 - 10M_{\odot}$ . This can be seen also from the evolutionary track of  $(r_{\text{a}}, \dot{M})$  in the  $10^{-4}Z_{\odot}$  panel of Figure 1. At  $\sim 0.1M_{\odot}$ , the track enters into the domain of instability, which is extended by the dust cooling toward lower accretion rate. When  $M_{*} > 10M_{\odot}$ , the decline of the accretion rate makes the disk stable again and the track exits from the domain of instability. In addition, as seen in the case of  $100M_{\odot}$ , temperature at the outer region  $\sim 1000\text{AU}$  is higher than inside because the dust cooling is only efficient in the inner dense region for  $M_{*} \gtrsim 10M_{\odot}$ . In this fashion, the outer disk becomes stable for those cases. In reality, however, the unstable disk with  $Q_{\text{T}} \sim 0.1$  would undergo catastrophic fragmentation before the stellar mass reaches  $10M_{\odot}$ . Once fragmentation occurs and multiple protostars are formed inside a single pre-stellar core, the infalling material will be shared among them. With reduced accretion rate onto individual protostars, the circumstellar disks around them would be finally stabilized (Sec.5.1).

Finally, we see the evolution of the  $Z = Z_{\odot}$  disk shown

in the right column of Figure 6. The outer radius of the disk is two or three orders of magnitude larger than the zero-metallicity one at the same stellar mass, reflecting the more extended envelope (bottom panel of Fig.5). The temperature is as low as  $10\text{K}$ , similar to the envelope value. This low disk temperature is due not only to efficient dust cooling but also to low heating rate because of the low accretion rate ( $\sim 10^{-6}M_{\odot}\text{yr}^{-1}$ ). In the inner disk of  $\lesssim 10\text{AU}$ , notwithstanding, the temperature jumps up to  $100 - 1000\text{K}$  owing to the large optical depth and to the deep potential well. As in the  $Z = 0$  case, the Toomre parameter is self-regulated to  $Q_{\text{T}} \simeq 1 - 1.5$ . As seen in the panel for the  $Z_{\odot}$  case in Figure 1, despite a larger domain of instability than in lower metallicity cases, the low value of accretion rate prevent the evolutionary track from entering it. Although the disk is predicted to become unstable in our model for  $M_{*} \gtrsim 10M_{\odot}$ , the stellar radiative heating would boost the disk temperature from  $\sim 10\text{K}$  in the case of such a massive star, and so our model would not be valid anymore. In addition, with accretion rate as low as  $10^{-6}M_{\odot}\text{yr}^{-1}$ , the star does not reach more massive than  $10M_{\odot}$  within its lifetime  $\lesssim 10\text{Myr}$ , and also, radiative pressure on the accretion flow can be important in halting the accretion (Larson & Starrfield 1971; Kahn 1974; Wolfire & Cassinelli 1987).

In Figure 7, the minimum values of Toomre parameter  $Q_{\text{T},\text{min}}$  in the disks are plotted as functions of the protostellar mass both for the fiducial rotation parameter  $f_{\text{Kep}} = 0.5$  (left) and for a smaller value  $0.25$  (right). First we see the



fiducial case. For the  $Z = 0$  and  $10^{-6}Z_{\odot}$  disks,  $Q_{T,\min}$  remains above unity until  $M_* = 20M_{\odot}$ . With metallicity of  $10^{-5} - 10^{-3}Z_{\odot}$ , the dust cooling becomes efficient enough to make the disks strongly unstable even in the early phase of  $M_* \lesssim 10M_{\odot}$ . In particular, the  $10^{-4}Z_{\odot}$  disk is most unstable with  $Q_{T,\min} \simeq 0.1$ . The sudden stabilization in this case at  $M_* \sim 10M_{\odot}$ , in which  $Q_{T,\min}$  jumps up to  $\simeq 1$ , is caused by the decline of accretion rate as mentioned previously. With more metals  $\gtrsim 10^{-2}Z_{\odot}$ , the disks are marginally stable  $Q_{T,\min} \gtrsim 1$  for the stellar mass below several solar masses. Next we see the case with slower rotation,  $f_{\text{Kep}} = 0.25$ . The disks are now smaller than in the fiducial case (eq.18). Due to higher temperature, disks are more stable at the inner radius. The smaller disks in the case of  $f_{\text{Kep}} = 0.25$  are thus more stable than those in the fiducial case. However, the trend that the disks with two extreme values of metallicity, i.e., either around  $Z = 0$  or  $Z = Z_{\odot}$ , are marginally stable while those with metallicity in between  $10^{-5} - 10^{-3}Z_{\odot}$  are strongly unstable are common in both cases.

We here consider physical reason why disks with  $10^{-5} - 10^{-3}Z_{\odot}$  are strongly unstable while those with higher and lower metallicity are relatively stable. Suppose a disk with temperature of  $T_{\text{disk}}$  is formed as a result of infall from an envelope with temperature  $T_{\text{env}}$ . From equations (15) and (16), the Toomre parameter of the disk can be written as

$$Q_{\text{T}} \simeq \frac{3\alpha c_s^3}{GM_{\text{env}}} \simeq 3\alpha \left( \frac{T_{\text{disk}}}{T_{\text{env}}} \right)^{3/2}. \quad (19)$$

Now suppose that the temperatures in the disk and in the envelope are similar,  $T_{\text{disk}} \simeq T_{\text{env}}$ . If the MRI always dominated the angular-momentum transfer ( $\alpha \ll 1$ ), the disk would become unstable with  $Q_{\text{T}} \ll 1$  from equation (19). In reality, once  $Q_{\text{T}}$  approaches unity, the gravitational torque becomes efficient and  $\alpha$  becomes close to unity. As a result, the disk is regulated to the marginally stable state of  $Q_{\text{T}} \gtrsim 1$ . On the other hand, if the disk temperature is less than  $\lesssim 1/2$  of the envelope temperature, the Toomre parameter is  $Q_{\text{T}} < 1$  even with the efficient angular-momentum transport  $\alpha = 1$ . Such a low-temperature disk cannot avoid fragmentation into pieces. Similar phenomenon has been reported by Kratter et al. (2010), who studied the evolution of rapidly accreting protostellar disks by way of isothermal hydrodynamic simulations and demonstrated that binary systems are formed by disk fragmentation if the accretion rate onto the disks  $\dot{M}_{\text{env}}$  exceeds  $3c_s^3/G$  (see also Kimura & Tsuribe 2012). In extremely low-metallicity ( $\lesssim 10^{-6}Z_{\odot}$ ) cases, the temperatures both in the envelope and in the disk have similar values of  $\simeq 1000\text{K}$  by the  $\text{H}_2$  cooling. The protostellar disks are (marginally) stable in those cases. With  $10^{-5} - 10^{-3}Z_{\odot}$ , on the other hand, the dust cooling operates only in dense environments in disks (see eq.12) and the disk temperature is  $\lesssim 100\text{K}$ , while the envelope temperature remains unaffected at several 100K. This disk/envelope temperature difference renders the protostellar disks strongly unstable. With metallicity exceeding  $10^{-2}Z_{\odot}$ , the disks become marginally stable again since the dust cooling is efficient both in the envelopes and disks. In summary, the protostellar disks are most unstable in the metallicity range of  $10^{-5} \lesssim Z/Z_{\odot} \lesssim 10^{-3}$  because of the difference in dominant coolants in the disks and envelopes.

This conclusion could be appropriate independently of the maximum  $\alpha$  value, although our results shown in this

section are obtained assuming  $\alpha_{\text{GI,max}} = 1$ . In Figure 2, we present the evolutionary tracks in  $r_{\text{d}} - \dot{M}$  planes for the maximum  $\alpha$  of 0.07 (Gammie 2001; Rice et al. 2005). Since the Toomre parameter is inversely proportional to  $\alpha$  (eq. 15 and 19), disks are more unstable than those with  $\alpha_{\text{GI,max}} = 1$ . However, we can also see that protostellar disks with  $10^{-5} - 10^{-3}Z_{\odot}$  are more unstable,  $Q_{\text{T}} \lesssim 0.1$  at  $0.1M_{\odot}$ , than zero and solar metallicity disks. Although the choice of the maximum  $\alpha$  value would alter the fragmentation boundary, it does not change the conclusion that the most unstable metallicity is  $10^{-5} \lesssim Z/Z_{\odot} \lesssim 10^{-3}$  (see also Sec. 5.2 and App. B).

## 5 DISCUSSION

### 5.1 Star formation at different metallicities

Based on our results, we here discuss plausible scenario for star formation at different metallicities. Our results indicate that star formation process with two extreme metallicities, i.e., at around zero- and the solar metallicity, is similar from the aspect of protostellar disk stability. The first stars are formed in minihalos of  $\sim 10^5 M_{\odot}$  at redshift  $z \sim 30$ , from parent pre-stellar cores of  $\sim 1000M_{\odot}$  formed by the  $\text{H}_2$ -line-induced fragmentation, and grows with accretion rate as high as  $10^{-3}M_{\odot} \text{ yr}^{-1}$  (e.g. Bromm & Larson 2004; Ciardi & Ferrara 2005; Glover 2013). The photoionizing feedback from the protostars eventually dissipates the materials in the envelopes and disks, thereby shutting off the accretion when the protostars reach  $\sim 100M_{\odot}$  (McKee & Tan 2008; Hosokawa et al. 2011; Stacy et al. 2012; Susa 2013; Tanaka et al. 2013; Hirano et al. 2013). On the other hand, in our Galaxy with metallicity of about the solar value, parent-core masses are typically  $\sim 1M_{\odot}$ , and the protostellar accretion rates are  $\sim 10^{-6}M_{\odot} \text{ yr}^{-1}$  (Shu et al. 1987; McKee & Ostriker 2007). While some envelope materials are expelled by magnetically driven protostellar outflow, the majority of parent-core gas is expected to be converted to the newborn star (Machida & Matsumoto 2012). In those ways, formation processes of the primordial and present-day stars look largely different in terms of the mass-scale and typical accretion rate. In both cases, nonetheless, the protostellar disks are self-regulated to a marginally stable state by the gravitational torque and would not go through catastrophic fragmentation (only modest one, if any), and most of the infalling gas is channelled onto the primary or a small number of multiple stars.

In low-metallicity environments with  $10^{-5} - 10^{-3}Z_{\odot}$ , massive clumps of  $100 - 1000M_{\odot}$  formed either by  $\text{H}_2$ , HD ( $\lesssim 10^{-4}Z_{\odot}$ ) or metal-line ( $\gtrsim 10^{-4}Z_{\odot}$ ) cooling are expected to fragment again at higher density by the dust cooling to form subsolar-mass pre-stellar cores. Some massive clumps, however, may fail to fragment in the dust cooling phase and survive due, for example, to lack of initial deformations or perturbations, or to small degree of rotation, etc. If so, two mass-scales of the pre-stellar cores,  $\gtrsim 100M_{\odot}$  and  $\lesssim 1M_{\odot}$ , may exist simultaneously. In the low-mass cores, all stars formed must be obviously low-mass. Even in the massive cores, our results indicate that low-mass stars can be formed by catastrophic disk fragmentation since protostellar disks with metallicity in this range are strongly unstable with

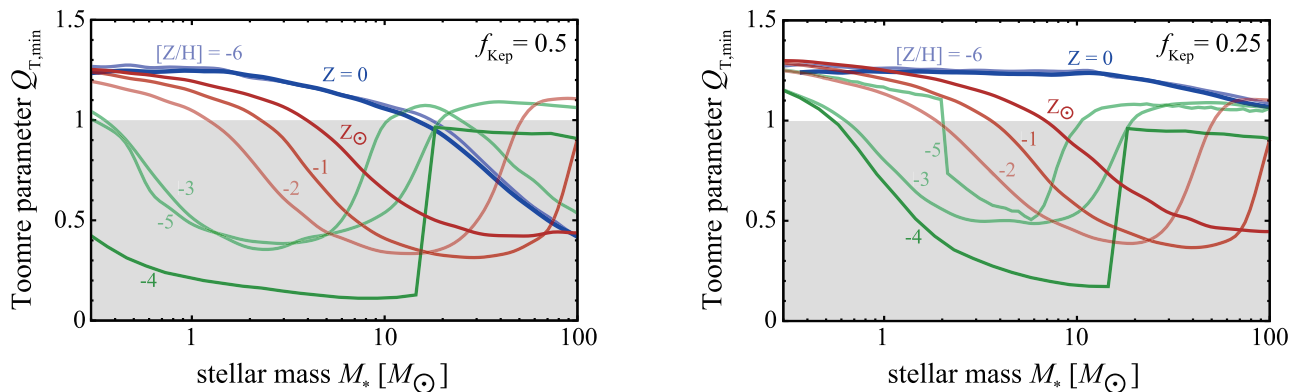


**Figure 7.** The evolution of the minimum Toomre parameter  $Q_{T,\min}$  in the disks with various metallicities  $Z/Z_\odot = 0, 10^{-6}$  (blue),  $10^{-5}, 10^{-4}, 10^{-3}$  (green),  $10^{-2}, 10^{-1}$ , and 1 (red) for the fiducial rotation parameter  $f_{\text{Kep}} = 0.5$  (left), and a smaller value  $f_{\text{Kep}} = 0.25$  (right). In the panels,  $[Z/H] = \log(Z/Z_\odot)$ . The horizontal axes indicate the mass of the protostar  $M_*$ , which grows in time.

$Q_T = 0.1 - 1$  (Sec. 4.2). The outcome would be a compact star-cluster, consisting of members of much lower-mass than the parent core. It should be noted that similar mechanism called the “fragmentation induced starvation” has been found to play a role in limiting the stellar mass in the context of present-day massive star formation (Peters et al. 2010). Our steady disk model cannot treat the evolution after the fragmentation, e.g., subsequent dynamical evolution of the resultant stellar system. We here try to estimate the mass and the number of stars formed by disk fragmentation. Recall that the Toomre parameter is roughly proportional to the accretion rate (see eq. 15). In the case of  $10^{-4}Z_\odot$ ,  $Q_T \simeq 0.1$  for the accretion rate  $\sim 10^{-4} - 10^{-3}M_\odot\text{yr}^{-1}$ . Therefore, once  $\sim 10$  stars are formed as a result of the fragmentation and the accretion flow is divided equally among them, the disk around each star would become marginally stable. On the other hand, the maximum stellar mass set by the photoionization feedback is about  $10M_\odot$  for this accretion rate (Hollenbach et al. 1994; Richling & Yorke 1997; Tanaka et al. 2013). Thus, even though the parent core is very massive  $> 100M_\odot$ , the end product would be a cluster of  $\gtrsim 10$  stars with mass less than  $10M_\odot$ . This mass scale has, in fact, also been suggested by observations of carbon enhanced metal-poor stars, whose frequency are known to increase with decreasing metallicity. Their possible origin is secondary stars in binary systems, enriched with carbon by mass transfer from the primary stars, which might have already evolved to white dwarfs by now. In this scenario, the typical mass of the primaries is considered to be a few  $M_\odot$  (Lucatello et al. 2005; Komiya et al. 2007; Suda et al. 2013). Our estimate above is concordance with this observational implication.

Although this coincidence is encouraging, with our simple model, we can treat neither detailed fragmentation process nor the subsequent dynamical evolution of fragments. Since typical distance between the fragments is as small as  $100 - 1000\text{AU}$ , some fragments may be scattered and/or merge with each other as a result of the gravitational interaction among them. In fact, even in the case of the metal-free star formation, some (although not many) low-mass fragments are found to be ejected from the system as a consequence of multi-body gravitational interactions (Clark et al.

2011; Vorobyov et al. 2013). More vigorous disk fragmentations are expected in low-metallicity environments with  $10^{-5} \lesssim Z/Z_\odot \lesssim 10^{-3}$ , and thus a larger number of fragments would be ejected before growing massive. This might be an origin of extremely metal-poor stars observed in the Galactic halo as well as of the free-floating planets. For quantitative predictions about nonlinear physics such as the disk fragmentation and the multi-body gravitational interaction, sophisticated numerical hydrodynamics including chemical and radiative processes are awaited.

The fragmentation of protostellar disks could produce very small objects with  $\lesssim 0.01M_\odot$ , or gas-giant planets, if with little accretion thereafter. In the metallicity range  $Z \sim Z_\odot$ , more fragmentation is expected in disks with lower metallicities from our results. On the other hand, observations find strong positive correlation between the discovery rate of giant exoplanets and the metallicity of host stars, with only few planets found in the range  $[\text{Fe}/\text{H}] < -0.5$  (Fischer & Valenti 2005; Mayor et al. 2011; Mortier et al. 2013). This is not in contradiction to our results as long as the dominant mechanism for giant-planet formation is not the gravitational fragmentation of the disks but the gas accretion onto the rocky cores. The disk fragmentation, however, might have produced the planet discovered recently around a metal-poor star of  $[\text{Fe}/\text{H}] \simeq -2$  (Setiawan et al. 2012) since large enough rocky cores to accrete gas are hard to form in such a low-metallicity environment (e.g., Johnson & Li 2012, 2013).

## 5.2 Uncertainties in our model

In the followings, we discuss uncertainties and effects not included in our model.

The uncertainty in the maximum value of  $\alpha$  is a significant problem to determine the fragmentation boundary. We mainly adopted  $\alpha_{\text{GI,max}} = 1$  as our reference value, which is supported by numerical simulations of star formation processes (Krumholz et al. 2007; Kratter et al. 2010; Clark et al. 2011; Kuiper et al. 2011). On the other hand, the isolated disk simulations suggest a smaller maximum  $\alpha$ . Gammie (2001) found that disks will fragment if the disk cooling time  $t_{\text{cool}} \simeq \Sigma c_s^2 / \gamma(\gamma - 1)\mathcal{L}$  is shorter than

$3\Omega_{\text{Kep}}^{-1}$  using local simulation, where  $\gamma$  is the adiabatic exponent. Since the cooling time can be rewritten as  $t_{\text{cool}} \simeq 4/9\gamma(\gamma - 1)\alpha\Omega_{\text{Kep}}$  (eq. 2, 4, 5, and 13) and Gammie (2001) assumed  $\gamma = 2$ , this result corresponds to the maximum  $\alpha$  value of 0.07. Rice et al. (2005) also supported  $\alpha_{\text{max}} = 0.07$  in the cases of  $\gamma = 5/3$  and  $7/5$  using the global simulation of isolated disks. This disagreement between star formation simulations and isolated disk simulations may be due to the numerical resolution. Recent higher resolution simulations of isolated disk demonstrated that fragmentation occurs even with much longer cooling timescale than  $3\Omega_{\text{Kep}}^{-1}$ , indicating the smaller  $\alpha_{\text{max}}$  (Meru & Bate 2011, 2012; Paardekooper et al. 2011). Paardekooper (2012) suggested the fragmentation is a stochastic process in the case of long cooling time and there are no certain boundary. Otherwise, this disagreement may be related to the mass ratio  $M_{\text{d}}/M_*$ . Since the infall supplies a large amount of gas onto the protostellar disk in star formation process, the disk mass keeps relatively high (Machida et al. 2010; Tsukamoto & Machida 2011) and the efficient mass redistribution is needed. Even in isolated disk simulations, Lodato & Rice (2005) showed that, if  $M_{\text{d}}/M_* \gtrsim 0.5$ , the large-scale structure ( $m = 2$  mode) induces the strong mass redistribution of  $\alpha > 0.1$  without fragmentation until settling down to quasi-steady state. In order to resolve this disagreement, high resolution simulations of star formation with realistic cooling processes are required. If the maximum value of  $\alpha$  is as small as 0.07 or less, the contribution of MRI has also non-negligible effect. The fixed  $\alpha_{\text{MRI}}$  of 0.01 is applied in this work. In reality, however, MRI activity depends on ionization degree. Especially, the existence of the dead zone where the MRI is not active by low ionization degree would be important in studying the entire disk evolution (Gammie 1996; Sano et al. 2000; Bai 2011). These uncertainties of  $\alpha$  description affects the fragmentation boundary. However, we would like to note that, even with this uncertainty, the protostellar disk at  $10^{-5} \lesssim Z/Z_{\odot} \lesssim 10^{-3}$  is quite unstable because the disk is  $Q_{\text{T}} \ll 1$  even with large value of  $\alpha_{\text{GI,max}} = 1$ . For the dependence of our results on the choice of  $\alpha$ , see also Appendix B.

In this work, we studied the disk structure using the steady mode ignoring temperature perturbation. For the solar metallicity case, Cossins et al. (2010) adopted a sophisticated fragmentation condition considering the cooling-rate dependence on temperature perturbation. The temperature perturbation leads some fraction of gas to have shorter cooling time than average, which accelerates fragmentation. They found that, at the temperature regime of ice or dust sublimation, the perturbation effect drops down the critical accretion rate for fragmentation about an order of magnitude from the value simply estimated by the average field. This effect may be important in low-metallicity star formation. For example, in the metallicity of  $10^{-4}Z_{\odot}$ , the protostellar disk at  $r \simeq 1\text{--}10\text{AU}$  has the dust sublimation temperature of about 1500K (Fig. 6). Although the average field is  $Q_{\text{T}} \gtrsim 1$ , fragmentation could be induced at this region by temperature perturbation. Therefore, it is an important topic for future works to clarify the details of the temperature-perturbation-induced instability in low-metallicity star formation.

We have adopted the same dust model as in the solar neighborhood. However, the dust property in the early

universe can be different. In particular, the depletion factor  $f_{\text{dep}}$ , i.e., the mass fraction of metals in the dust phase, affects significantly the dust cooling rate (Schneider et al. 2012). The dust grains in the early universe are considered to be produced in supernovae, and destructed by the reverse shocks. The resultant depletion factor is typically a few percent, depending on the ambient density, much smaller than in the solar neighborhood ( $f_{\text{dep}} \simeq 0.5$ ) (Nozawa et al. 2007). Recent studies by Nozawa et al. (2012) and Chiaki et al. (2013), however, showed that, even though  $f_{\text{dep}} \ll 1$  initially, the dust grains could grow during the pre-stellar collapse owing to the sticking of silicate particles onto the dust, thereby boosting the depletion factor to the order of unity. Since the protostellar disks are dense enough for the dust growth to work, our adoption of the Galactic value of  $f_{\text{dep}} \sim 1$  would be justified.

As the disk heating mechanism, we have considered only the viscous heating. Also the radiative heating from the central star, however, can be important and stabilize the disks in some circumstances. The degree of the stellar radiative heating depends on whether the innermost part of the disk is puffed up or not: if so, the outer disk is effectively shielded from the stellar radiation (see Dullemond et al. 2001). In fact, our result for  $10M_{\odot}$  at  $10^{-4}Z_{\odot}$  shows that the aspect ratio  $H/r = 0.2$  at 1AU, while  $H/r = 0.06$  at 100AU. Although the innermost disk of 1AU could be geometrically thick due to high temperature there, we estimate the stellar heating without the shadowing as the conservative upper limit. The equilibrium disk temperature  $T_{\text{irr}}$  determined by the balance between the stellar heating and the radiative cooling is

$$T_{\text{irr}} \simeq 74 \left( \frac{M_*}{M_{\odot}} \right)^{-1/7} \left( \frac{L_*}{10^3 L_{\odot}} \right)^{2/7} \left( \frac{r}{100\text{AU}} \right)^{-3/7} \text{K}, \quad (20)$$

where  $L_*$  is the bolometric stellar luminosity (Kusaka et al. 1970; Chiang & Goldreich 1997). In evaluating  $T_{\text{irr}}$ , we use  $L_*$  from Hosokawa & Omukai (2009), who calculated the protostellar evolution for various metallicities. For metallicity lower than  $\sim 10^{-3}Z_{\odot}$ , the stellar heating has little influence on the disk because the temperature determined by the viscous heating is already high with 100 – 1000K. On the other hand, for  $\gtrsim 10^{-2}Z_{\odot}$ , the temperature by the viscous heating being only  $\sim 10\text{K}$ , the stellar heating can be important unless the shadowing is effective (see also Omukai et al. 2010). For the solar-metallicity disks, the importance of stabilization by the stellar radiation heating has already been pointed out by Matzner & Levin (2005); Cai et al. (2008). As seen in Section 4.2, the protostellar disks with  $\gtrsim 10^{-2}Z_{\odot}$  are already relatively stable only with the viscous heating and the additional heating by the stellar radiation will just make them even more stable. We thus conclude that the stellar-heating stabilization does not qualitatively alter the general trend of disk-stability dependence on the metallicity.

## 6 CONCLUSION

We have calculated the structure of protostellar disks with various metallicities by the steady-state  $\alpha$ -disk models, and examined their stability against self-gravity by the Toomre  $Q_{\text{T}}$  value. By constructing the envelope structure from the thermal evolution during the preceding collapse phase, the

accretion rate onto the disk is evaluated as  $\propto T_{\text{env}}^{3/2}$ , where  $T_{\text{env}}$  is the envelope temperature. In this case,  $Q_{\text{T}}$  can be written using the ratio of the temperatures in the disk and in the envelope as  $\sim \alpha_{\text{max}}(T_{\text{disk}}/T_{\text{env}})^{3/2}$ . Here  $\alpha_{\text{max}}$  is the maximum value of the viscous parameter  $\alpha$ , which is about unity. We have found that the protostellar disks can be classified into the following three metallicity regimes according to the disk stability, which is determined by the ratio  $T_{\text{disk}}/T_{\text{env}}$ .

(i) extremely low-metallicity ( $\lesssim 10^{-6}Z_{\odot}$ ) disks: Both in the envelope and in the disk, the temperature is  $\sim 1000\text{K}$  by the  $\text{H}_2$ -line cooling. The disk is self-regulated to marginally stable state,  $Q_{\text{T}} \simeq 1$ , by the gravitational torque.

(ii) very low-metallicity ( $10^{-5}$ – $10^{-3}Z_{\odot}$ ) disks: Temperature in the disk is  $\sim 100\text{K}$  by the dust cooling due to its high density  $\gtrsim 10^{10}\text{cm}^{-3}$ , while in the envelope it is several 100K by the  $\text{H}_2$ , HD ( $\lesssim 10^{-4}Z_{\odot}$ ) or metal-line cooling ( $\gtrsim 10^{-4}Z_{\odot}$ ). This temperature difference results in a strongly unstable disk with  $Q_{\text{T}} \sim 0.1$ , which is destined to fragment catastrophically.

(iii) metal-enriched ( $\gtrsim 10^{-2}Z_{\odot}$ ) disks: Temperatures are about 10K both in the envelope and the disk by efficient dust cooling. As in the extremely low-metallicity case, the disk is regulated to marginally stable state of  $Q_{\text{T}} \simeq 1$ .

In the extremely metal-poor and metal-enriched environments, only the modest fragmentation of protostellar disks is expected. Therefore, most of the infalling material would accrete onto the primary or a small number of multiple stars. The typical mass of stars would be limited either by the available reservoir set by the parental core mass in the metal-enriched case (at  $\sim 0.1 - 1M_{\odot}$ ) or by radiative feedbacks in the extremely metal-poor case (at  $\sim 100M_{\odot}$ ).

In the low-metallicity environment of  $10^{-5}$ – $10^{-3}Z_{\odot}$ , two mass-scales of parent cores may co-exist with  $\lesssim 1M_{\odot}$  and  $\gtrsim 100M_{\odot}$ . The low-mass and high-mass cores are, respectively, formed by dust-cooling and line-cooling induced fragmentation during the pre-stellar collapse phase. Since the disks in this metallicity range are highly unstable, even in massive cores, low-mass stars would be formed by the protostellar disk fragmentation. Those stars would grow as massive as  $\sim 10M_{\odot}$  or less, depending on complex interplay between multi-body gravitational interaction, gas accretion, and stellar radiative feedbacks. This is roughly consistent with inferred mass-scale of metal-poor stars from observations of carbon-enhanced metal-poor stars in the Galactic halo (Lucatello et al. 2005; Komiya et al. 2007; Suda et al. 2013).

In conclusion, the fragmentation of the protostellar disks by the dust cooling, in cooperation with that during the pre-stellar collapse, accelerates the transition from massive to low-mass star formation mode at the critical metallicity around  $Z_{\text{crit}} \simeq 10^{-5}Z_{\odot}$ .

## ACKNOWLEDGMENTS

The authors thank Eduard Vorobyov, Raffaella Schneider, Masahiro N. Machida, Takashi Hosokawa, Satoshi Okuzumi, Kengo Tomida, Yusuke Tsukamoto, Kohei Inayoshi and Sanemichi Takahashi for fruitful discussions and comments. The authors also thank the anonymous referee for com-

ments, which were useful to improve the original manuscript. This work is supported by the Grants-in-Aid by the Ministry of Education, Science and Culture of Japan (KO: 21684007, 25287040).

## APPENDIX A: CRITICAL DENSITY FOR THERMAL COUPLING OF GAS AND DUST

Here we find the threshold density  $n_{\text{H,tc}}$  above which the gas and dust are thermally coupled (eq. 12). As shown in Figure 3, the dust temperature falls short of the gas temperature while dust cooling is not efficient. Those temperatures become almost equal soon after the dust cooling dominates.

Suppose now that  $T_{\text{d}} \ll T$ , i.e., before the thermal coupling, and the dust cooling is still inefficient. In this case, the disks are optically thin and the radiation temperature  $T_{\text{rad}} (\simeq \tau_{\text{T}} T_{\text{d}}; \text{eq. 11})$  is even smaller than  $T_{\text{d}}$ . The dust temperature  $T_{\text{d}}$  is determined by the thermal equilibrium for the dust grains (eq. 10). Writing the mean free time for the gas-dust collision using the dust cross-section  $\sigma_{\text{d}}$  as

$$t_{\text{coll}} = (\sigma_{\text{d}} \bar{n} \bar{v})^{-1}, \quad (\text{A1})$$

where  $\bar{n} \bar{v}$  is the number density multiplied by velocity averaged over colliding particles (Hollenbach & McKee 1979; Schneider et al. 2006, 2012), the thermal equilibrium (eq. 10) reads

$$4\sigma_{\text{SB}} \rho \kappa_{\text{d,P}} T_{\text{d}}^4 = 2k_{\text{B}} T n_{\text{d}} \sigma_{\text{d}} \bar{n} \bar{v}, \quad (\text{A2})$$

where we have omitted the terms related to  $T_{\text{rad}}$  on the left-hand side and  $T_{\text{d}}$  on the right-hand side. The opacity  $\kappa_{\text{d,P}}$  and the total cross-section of grains per unit gas mass  $n_{\text{d}} \sigma_{\text{d}} / \rho$  are taken from the Semenov et al. (2003)'s model and are approximately written as

$$\kappa_{\text{d,P}} \simeq 7.4 \left( \frac{Z}{Z_{\odot}} \right) \left( \frac{T_{\text{d}}}{100\text{K}} \right)^2 \text{ cm}^2 \text{ g}^{-1}, \quad (\text{A3})$$

$$n_{\text{d}} \sigma_{\text{d}} / \rho \simeq 470 \left( \frac{Z}{Z_{\odot}} \right) \text{ cm}^2 \text{ g}^{-1}, \quad (\text{A4})$$

with errors less than 20% for  $T_{\text{d}} = 10 - 100\text{K}$ . Substituting them into equation (A2), we obtain

$$T_{\text{d}} \simeq 59 \left( \frac{T}{100\text{K}} \right)^{1/4} \left( \frac{n_{\text{H}}}{10^{10}\text{cm}^{-3}} \right)^{1/6} \text{ K}. \quad (\text{A5})$$

The dust temperature  $T_{\text{d}}$  depends only explicitly on the gas temperature  $T$  and density  $n_{\text{H}}$ , but not on the metallicity  $Z$ . Note, however, that the dependence on  $Z$  comes through the gas temperature, which depends on  $Z$ . Equating  $T_{\text{d}}$  with  $T$  in equation (A5), we can evaluate the density where the gas and dust thermally couple:

$$n_{\text{H,tc}} \simeq 2.3 \times 10^{11} \left( \frac{T}{100\text{K}} \right)^{4.5} \text{ cm}^{-3}. \quad (\text{A6})$$

This value agrees well with our results and also results for collapsing cloud calculation by Omukai (2000).

## APPENDIX B: DEPENDENCE ON VISCOUS PARAMETER

As we stated in Section 5.2, the prescription of  $\alpha$  parameter has uncertainty. Therefore, we here demonstrate the robustness and sensitivity of our results to the value of  $\alpha$ .

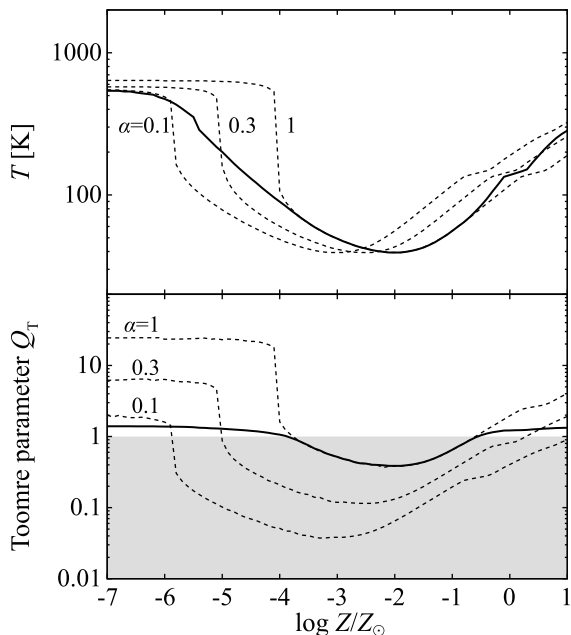


**Figure B1.** Comparison of the results with variable and constant  $\alpha$ 's. The temperature (*top*) and the Toomre parameter (*bottom*) as functions of metallicity are shown for  $M_* = 10M_\odot$ ,  $\dot{M} = 10^{-4}M_\odot \text{ yr}^{-1}$ , and  $r = 100\text{AU}$ . *Solid*: the case with the variable  $\alpha$  ( $= \exp(-Q_T^{10}/10) + 10^{-2}$ ) used in the main part of this paper, *dashed*: the cases with constant  $\alpha$  values ( $\alpha = 0.1, 0.3,$  and  $1$ ).

Figure B1 shows the temperature  $T$  (*top*) and the Toomre parameter  $Q_T$  (*bottom*) for models with our variable and three constant  $\alpha$  values (here we fix  $M_* = 10M_\odot$ ,  $\dot{M} = 10^{-4}M_\odot \text{ yr}^{-1}$ , and  $r = 100\text{AU}$ ). In all cases, the metallicity dependence of temperature is qualitatively similar: the temperature is lowest at 30K around  $10^{-3}$ – $10^{-2}Z_\odot$ , while it is as high as several hundred kelvin at either higher or lower metallicities. On the other hand, the value of Toomre parameter  $Q_T$  changes in response to the choice of the  $\alpha$  value. The  $Q_T$  value is approximately proportional to  $\alpha$  in the constant  $\alpha$  cases (see also eq. 15), while, in the case of the variable  $\alpha$ , it remains  $Q_T \simeq 1$  for a wide range of metallicity due to the regulation by the gravitational torque, which is effective only if  $Q_T \lesssim 1.5$ . Since the maximum  $\alpha$  is set to unity in the variable  $\alpha$  case, the result in this case coincides with that with  $\alpha = 1$  when  $Q_T < 1$ . Although the value of  $Q_T$  itself changes with the choice of  $\alpha$ , the tendency that it is lowest around  $10^{-3}$ – $10^{-2}Z_\odot$  is common in all cases. This fact confirms the robustness of our conclusion that the protostellar disks with  $10^{-5}$ – $10^{-3}Z_\odot$  are the most unstable.

## REFERENCES

- Abel, T., Bryan, G. L., & Norman, M. L. 2002, *Science*, 295, 93
- Bai, X.-N. 2011, *ApJ*, 739, 50
- Bate, M. R. 1998, *ApJ*, 508, L95
- Bromm, V., Ferrara, A., Coppi, P. S., & Larson, R. B. 2001, *MNRAS*, 328, 969
- Bromm, V., & Larson, R. B. 2004, *ARA&A*, 42, 79
- Bromm, V., & Loeb, A. 2004, *Nature*, 9, 353
- Boley, A. C., Mejía, A. C., Durisen, R. H., et al. 2006, *ApJ*, 651, 517
- Boss, A. P. 2002, *ApJ*, 567, L149
- Bromm, V., & Loeb, A. 2003, *Nature*, 425, 812
- Cai, K., Durisen, R. H., Boley, A. C., Pickett, M. K., & Mejía, A. C. 2008, *ApJ*, 673, 1138
- Cai, K., Durisen, R. H., Michael, S., et al. 2006, *ApJ*, 636, L149
- Chabrier, G. 2003, *PASP*, 115, 763
- Chiaki, G., Nozawa, T., & Yoshida, N. 2013, *ApJ*, 765, L3
- Chiang, E. I., & Goldreich, P. 1997, *ApJ*, 490, 368
- Ciardi, B., & Ferrara, A. 2005, *Space Sci. Rev.*, 116, 625
- Clark, P. C., Glover, S. C. O., & Klessen, R. S. 2008, *ApJ*, 672, 757
- Clark, P. C., Glover, S. C. O., Smith, R. J., et al. 2011, *Science*, 331, 1040
- Clarke, C. J. 2009, *MNRAS*, 396, 1066
- Cossins, P., Lodato, G., & Clarke, C. J. 2009, *MNRAS*, 393, 1157
- Cossins, P., Lodato, G., & Clarke, C. 2010, *MNRAS*, 401, 2587
- Davis, S. W., Stone, J. M., & Pessah, M. E. 2010, *ApJ*, 713, 52
- Dullemond, C. P., Dominik, C., & Natta, A. 2001, *ApJ*, 560, 957
- Dopcke, G., Glover, S. C. O., Clark, P. C., & Klessen, R. S. 2011, *ApJ*, 729, L3
- Dopcke, G., Glover, S. C. O., Clark, P. C., & Klessen, R. S. 2013, *ApJ*, 766, 103
- Fischer, D. A., & Valenti, J. 2005, *ApJ*, 622, 1102
- Gammie, C. F. 1996, *ApJ*, 457, 355
- Gammie, C. F. 2001, *ApJ*, 553, 174
- Glover, S. 2013, *Astrophysics and Space Science Library*, 396, 103
- Hirano, S., Hosokawa, T., Yoshida, N., et al. 2013, arXiv:1308.4456
- Hollenbach, D., Johnstone, D., Lizano, S., & Shu, F. 1994, *ApJ*, 428, 654 (HJLS94)
- Hollenbach, D., & McKee, C. F. 1979, *ApJS*, 41, 555
- Hosokawa, T., & Omukai, K. 2009, *ApJ*, 703, 1810
- Hosokawa, T., Omukai, K., Yoshida, N., & Yorke, H. W. 2011, *Science*, 334, 1250
- Johnson, J. L., & Li, H. 2012, *ApJ*, 751, 81
- Johnson, J. L., & Li, H. 2013, *MNRAS*, 431, 972
- Kahn, F. D. 1974, *A&A*, 37, 149
- Kimura, S. S., & Tsuribe, T. 2012, *PASJ*, 64, 116
- Komiya, Y., Suda, T., Minaguchi, H., et al. 2007, *ApJ*, 658, 367
- Kratter, K. M., Matzner, C. D., & Krumholz, M. R. 2008, *ApJ*, 681, 375
- Kratter, K. M., Matzner, C. D., Krumholz, M. R., & Klein, R. I. 2010, *ApJ*, 708, 1585
- Kroupa, P. 2002, *Science*, 295, 82
- Krumholz, M. R., Klein, R. I., McKee, C. F., Offner, S. S. R., & Cunningham, A. J. 2009, *Science*, 323, 754
- Krumholz, M. R., Stone, J. M., & Gardiner, T. A. 2007, *ApJ*, 671, 518
- Kuiper, R., Klahr, H., Beuther, H., & Henning, T. 2011, *ApJ*, 732, 20
- Kusaka, T., Nakano, T., & Hayashi, C. 1970, *Progress of Theoretical Physics*, 44, 1580

- Larson, R. B. 1969, MNRAS, 145, 271
- Larson, R. B., & Starrfield, S. 1971, A&A, 13, 190
- Lin, D. N. C., & Pringle, J. E. 1987, MNRAS, 225, 607
- Lodato, G., & Rice, W. K. M. 2004, MNRAS, 351, 630
- Lodato, G., & Rice, W. K. M. 2005, MNRAS, 358, 1489
- Lucatello, S., Tsangarides, S., Beers, T. C., et al. 2005, ApJ, 625, 825
- Machida, M. N., Inutsuka, S.-i., & Matsumoto, T. 2010, ApJ, 724, 1006
- Machida, M. N., & Matsumoto, T. 2012, MNRAS, 421, 588
- Matzner, C. D., & Levin, Y. 2005, ApJ, 628, 817
- Mayer, M., & Duschl, W. J. 2005, MNRAS, 358, 614
- Mortier, A., Santos, N. C., Sousa, S., et al. 2013, A&A, 551, A112
- McKee, C. F., & Ostriker, E. C. 2007, ARA&A, 45, 565
- McKee, C. F., & Tan, J. C. 2008, ApJ, 681, 771
- Meru, F., & Bate, M. R. 2010, MNRAS, 406, 2279
- Meru, F., & Bate, M. R. 2011, MNRAS, 411, L1
- Meru, F., & Bate, M. R. 2012, MNRAS, 427, 2022
- Mayor, M., Marmier, M., Lovis, C., et al. 2011, arXiv:1109.2497
- Nakamoto, T., & Nakagawa, Y. 1994, ApJ, 421, 640
- Nakamoto, T., & Nakagawa, Y. 1995, ApJ, 445, 330
- Nozawa, T., Kozasa, T., Habe, A., et al. 2007, ApJ, 666, 955
- Nozawa, T., Kozasa, T., & Nomoto, K. 2012, ApJ, 756, L35
- Omukai, K. 2000, ApJ, 534, 809
- Omukai, K. 2001, ApJ, 546, 635
- Omukai, K. 2012, PASJ, 64, 114
- Omukai, K., & Nishi, R. 1998, ApJ, 508, 141
- Omukai, K., Hosokawa, T., & Yoshida, N. 2010, ApJ, 722, 1793
- Omukai, K., Tsuribe, T., Schneider, R., & Ferrara, A. 2005, ApJ, 626, 627
- Paardekooper, S.-J. 2012, MNRAS, 421, 3286
- Paardekooper, S.-J., Baruteau, C., & Meru, F. 2011, MNRAS, 416, L65
- Peters, T., Klessen, R. S., Mac Low, M.-M., & Banerjee, R. 2010, ApJ, 725, 134
- Pringle, J. E. 1981, ARA&A, 19, 137
- Rice, W. K. M., & Armitage, P. J. 2009, MNRAS, 396, 2228
- Rice, W. K. M., Armitage, P. J., Bate, M. R., & Bonnell, I. A. 2003, MNRAS, 339, 1025
- Rice, W. K. M., Lodato, G., & Armitage, P. J. 2005, MNRAS, 364, L56
- Richling, S., & Yorke, H. W. 1997, A&A, 327, 317
- Sano, T., Miyama, S. M., Umebayashi, T., & Nakano, T. 2000, ApJ, 543, 486
- Schneider, R., Ferrara, A., Natarajan, P., & Omukai, K. 2002, ApJ, 571, 30
- Schneider, R., Ferrara, A., Salvaterra, R., Omukai, K., & Bromm, V. 2003, Nature, 422, 869
- Schneider, R., Omukai, K., Bianchi, S., & Valiante, R. 2012, MNRAS, 419, 1566
- Schneider, R., Omukai, K., Inoue, A. K., & Ferrara, A. 2006, MNRAS, 369, 1437
- Semenov, D., Henning, T., Helling, C., Ilgner, M., & Sedlmayr, E. 2003, A&A, 410, 611
- Setiawan, J., Roccatagliata, V., Fedele, D., et al. 2012, A&A, 540, A141
- Shakura, N. I., & Sunyaev, R. A. 1973, A&A, 24, 337
- Shi, J., Krolik, J. H., & Hirose, S. 2010, ApJ, 708, 1716
- Shu, F. H. 1977, ApJ, 214, 488
- Shu, F. H., Adams, F. C., & Lizano, S. 1987, ARA&A, 25, 23
- Stacy, A., & Bromm, V. 2013, MNRAS, 1469
- Stacy, A., Greif, T. H., & Bromm, V. 2010, MNRAS, 403, 45
- Stacy, A., Greif, T. H., & Bromm, V. 2012, MNRAS, 422, 290
- Stahler, S. W., Palla, F., & Salpeter, E. E. 1986, ApJ, 302, 590
- Stahler, S. W., Shu, F. H., & Taam, R. E. 1980, ApJ, 241, 637
- Suda, T., Komiya, Y., Yamada, S., et al. 2013, MNRAS, 432, L46
- Susa, H. 2013, ApJ, 773, 185
- Takahashi, S. Z., Inutsuka, S.-i., & Machida, M. N. 2013, ApJ, 770, 71
- Tan, J. C., & McKee, C. F. 2004, ApJ, 603, 383
- Tanaka, K. E. I., & Nakamoto, T. 2011, ApJ, 739, L50
- Tanaka, K. E. I., Nakamoto, T., & Omukai, K. 2013, ApJ, 773, 155
- Toomre, A. 1964, ApJ, 139, 1217
- Tsukamoto, Y., & Machida, M. N. 2011, MNRAS, 416, 591
- Vorobyov, E. I., & Basu, S. 2010, ApJ, 719, 1896
- Vorobyov, E. I., DeSouza, A. L., & Basu, S. 2013, ApJ, 768, 131
- Walch, S., Burkert, A., Whitworth, A., Naab, T., & Gritschneider, M. 2009, MNRAS, 400, 13
- Wolfire, M. G., & Cassinelli, J. P. 1987, ApJ, 319, 850
- Yoshida, N., Omukai, K., Hernquist, L., & Abel, T. 2006, ApJ, 652, 6
- Zhu, Z., Hartmann, L., Gammie, C., & McKinney, J. C. 2009, ApJ, 701, 620
- Zinnecker, H., & Yorke, H. W. 2007, ARA&A, 45, 481

This paper has been typeset from a  $\text{\TeX}$ / $\text{\LaTeX}$  file prepared by the author.